The Cryosphere Discuss., https://doi.org/10.5194/tc-2018-128
Manuscript under review for journal The Cryosphere
Discussion started: 7 August 2018

The Cryosphere Discussions
Open Access
EGU

Long-range terrestrial laser scanning measurements of summer and annual mass balances for Urumqi Glacier No.1, eastern Tien Shan, China

Chunhai Xu[1, 2], Zhongqin Li[1*], Huilin Li[1, 2], Feiteng Wang[1], and Ping Zhou[1]

[1] State Key Laboratory of Cryospheric Science/Tien Shan Glaciological Station, Northwest Institute of Eco-Environment and Resources, Chinese Academy of Sciences, Lanzhou 730000, China

[2] University of Chinese Academy of Sciences, Beijing 100049, China

Correspondence to: Zhongqin Li (lizq@lzb.ac.cn)

Abstract. The direct glaciological method typically provides in situ observations of annual or seasonal surface mass balance, but can only be implemented through a succession of intensive in situ measurements of measuring networks of stakes and snow pits. This has contributed to glacier surface mass-balance measurements being sparse and often discontinuous in the Tien Shan. Nevertheless, long-term glacier mass-balance measurements are the basis for understanding climate–glacier interactions and projecting future water availability for glacierized catchments in the Tien Shan. Riegl VZ®-6000 long-range terrestrial laser scanning (TLS), typically using class 3B laser beams, is exceptionally well suited for measuring snowy and icy terrain in repeated glacier mapping, and subsequently annual and seasonal geodetic mass balance can be determined. This paper introduces the applied TLS for monitoring summer and annual surface elevation and geodetic mass changes of Urumqi Glacier No.1 (UG1) as well as delineating accurate glacier boundaries for two consecutive years (2015-17), and discusses the potential of such technology in glaciological applications. Three-dimensional changes of ice and firn/snow bodies and the corresponding densities were considered for the volume-to-mass conversion. UG1 showed pronounced thinning and mass loss for the four investigated periods; glacier-wide geodetic mass balance in the mass-balance year 2015-16 was slightly more negative than in 2016-17. The majority of TLS-derived geodetic elevation changes at individual stakes were slightly positive, but showed a close correlation with the glaciological elevation changes (changes in exposed stake height) of individual stakes ($R^2 \geq 0.90$). Statistical comparison shows that agreement between the glaciological and geodetic mass balances can be considered satisfying, indicating that the TLS system yields accurate results and has the potential to monitor remote and inaccessible glacier areas where no glaciological measurements are available.

1. Introduction

Glacier meltwater is a crucial freshwater resource for populations and hydro-economies in arid and semi-arid regions (e.g. Sorg et al., 2012; Chen et al., 2016). The function known as ‘solid reservoirs’ is well represented in the Tien Shan, where most glaciers have experienced substantial mass loss over recent decades (Farinotti et al., 2015; Pieczonka et al., 2015; Liu et al., 2016; Sakai et al., 2017; Li et al., 2018). Hence, a better understanding of the relationship between Tien Shan glacier wastage and changing climate is important for projecting water availability in the near future. Glacier mass balance provides important information on the gain or loss in glacier mass and is a direct and immediate indicator of climate evolution (Kaser et al., 2006; Haeberli et al., 2007).

Ongoing mass-balance observations are fundamental to understand climate–glacier interactions (Zemp et al., 2015). Annual and sometimes seasonal surface mass balance of individual glaciers can be measured using the direct glaciological method. Stakes are

drilled into the ice, allowing the monitoring of ablation, and snow pits are dug in the area where snow has accumulated to provide net accumulation (Østrem and Brugman, 1991; Xie et al., 1991; Cogley et al., 2011). However, the shortage of long-term financial and human resources and the inaccessibility of remote regions and natural hazards means that ongoing in situ glacier mass-balance measurements are sparse in the Tien Shan, so that only Tuyuksu glacier (northern Tien Shan, Kazakhatan) and Urumqi Glacier No.1 (eastern Tien Shan, China) have long glaciological mass balance series (Hoelzle et al., 2017). In contrast to the extensive in situ measurement networks required for glaciological observations, the geodetic method provides mass balance by repeated surveys of the entire glacier surface terrain, in which two digital elevation models (DEMs) are subtracted to calculate the volume changes and then convert them to mass balance using a density conversion (Zemp et al., 2013; Huss, 2013; Andreassen et al., 2016). The method measures all processes that induce the surface, internal and basal mass balances (Cuffey and Paterson, 2010; Sold et al., 2016) but the geodetic mass balances are assumed to be accurate since the topographic surveys are of high quality (Thibert et al., 2008; Huss et al., 2009; Joerg et al., 2012). The available DEMs, derived from aerial photography and traditional remote sensing imagery, usually limit the accuracy and spatiotemporal resolution of geodetic mass-balance measurements (e.g. Cox and March et al., 2004; Cogley, 2009; Fischer, 2011).

In recent years, burgeoning earth observation technologies (e.g. airborne (ALS) and terrestrial laser scanning (TLS)), which allow the derivation of high-resolution DEMs with vertical and horizontal errors on the order of a few centimeters, have increasingly been used to calculate glacier volume and geodetic mass changes (e.g. Kerr et al., 2009; Abermann et al., 2010; Fischer, 2011; Joerg et al., 2012; Gabbud et al., 2015; Andreassen et al., 2016; Fischer et al., 2016; López-Moreno et al., 2016; Xu et al., 2017; Klug et al., 2018). ALS is advantageous for rapidly mapping wide areas, but the high costs, the difficulty of studying small-scale processes, and the presence of rock outcrops limit the capacity of observations by aircraft and require ground-based surveys (Young et al., 2010; Piermattei et al., 2015). The TLS system is usually simpler, more economical and more flexible than ALS, and has became a well-established tool for monitoring annual and sometimes seasonal evolutions of individual glaciers (e.g. Gabbud et al., 2015; Fischer et al., 2016; López-Moreno et al., 2016), reference glaciers in particular. The new high-speed and -resolution Riegl VZ®-6000 terrestrial laser scanner offers a long measurement range of more than 6 km and a wide field of 60 °vertical and 360 °horizontal for topographic (static) applications (RIEGL Laser Measurement Systems, 2014a). Being the Laser Class 3B, it is, due to its laser wavelength in the near-infrared (~1064 nm), exceptionally well suited for measuring snow- and ice-covered terrains in repeated glacier mapping. Some recent studies have covered the novel use of Riegl VZ®-6000 TLS to measure surface melt for a temperate Alpine valley glacier at the seasonal and hourly scales (Gabbud et al., 2015); however, only the central and bottom portions of the glacier were detected. Others present the performance of Riegl VZ®-6000 in monitoring the mass balance of five glaciers in the European Alps; the surface terrain of each glacier can be almost entirely detected using one scan position since these glaciers are very small and their terrains are steep (Fischer et al., 2016). For medium-sized and large reference glaciers with flat terrain, however, a single scan position cannot capture the whole glacier surface.

Urumqi Glacier No.1 (hereafter known as UG1) is the best-monitored glacier in China. It is also one of the reference glaciers in the World Glacier Monitoring Service (WGMS) network due to its long-term data series, important location and significant local water supply (Li et al., 2011; Zemp et al., 2009). Riegl VZ®-6000 TLS surveys of UG1 were initiated on 25 April 2015 for four scan positions (Fig. 1a), and the subsequent measurements were nearly coincident with days of glaciological measurements. Multi-temporal high-resolution and -precision TLS-derived DEMs are therefore available. To date, a geodetic reanalysis of seasonal and annual glaciological mass balance of UG1 has not received attention. Comparison of glaciological and geodetic mass balances of UG1 was only reported for the period 1981-2009 at intervals of several years (Wang et al., 2014). Our previous studies have used

The Cryosphere Discuss., https://doi.org/10.5194/tc-2018-128
Manuscript under review for journal The Cryosphere
Discussion started: 7 August 2018

the TLS to monitor the net mass balance of UG1 at the monthly scale (25 April-28 May 2015), whereas we simply compared glaciological and TLS-derived geodetic elevation changes of individual stakes, whether agreement between the glaciological and TLS-derived glacier-wide mass balance was pending, potential of such technology applied in seasonal and annual glacier mass-balance measurements in western China had not been discussed; besides we only considered snow/firn densities in the geodetic mass balance calculations as an abundance of fresh snow covered the entire glacier surface at the time of the TLS surveys (Xu et al., 2017). In fact, a density conversion of volume changes to mass balance becomes more challenging over short time periods because of meteorological influences on the elevation changes (Huss, 2013). Some studies use the volume-weighting method to calculate the annual conversion density by classifying a glacier surface into bare ice and firn (e.g. Fischer et al., 2016; Klug et al., 2018). However, the volume changes in ice and firn/snow usually take place at the same vertical layer for summer-accumulation-type glaciers (accumulation and ablation take part simultaneously in summer months) according to our field observations, so we cannot classify ice and firn using remotely sensed methods in this study. Besides, compaction and metamorphosis imply a shift in the vertical firn profile as well as changes in firn thickness and density (Cuffey and Paterson, 2010; Ligtenberg et al., 2011).

Hence, the aims of the present study are: (1) to describe the original use of Riegl VZ®-6000 TLS-derived DEMs to calculate summer and annual geodetic mass balances of UG1 for two consecutive years (2015-17); (2) to consider three-dimensional (3-D) changes of ice and firn/snow bodies and density conversion from in situ measured snow/firn densities is applied to make these calculations. Firn compaction and metamorphosis can be therefore captured to some extent; (3) to compare the geodetic results to glaciological glacier-wide mass balances through a detailed uncertainty assessment of the glaciological and geodetic methods; (4) to discuss how to achieve good quality of point cloud data and DEM differencing and to analyze the possible cause of the difference between the two methods; and (5) to take UG1 as a case to assess the potential of such long-range TLS to measure glacier mass balance at the seasonal and annual scales and put forward some main considerations for a broader application of the TLS.

2. Study site

UG1 is a northeast-orientated valley glacier, situated on the northern slope of Tianger Summit II (4848 m a.s.l.) in the eastern Tien Shan (43°06′N, 86°49′E, Fig. 1a and b), and consists of two independent small glaciers: the east branch (EB) and the west branch (WB). UG1 covered a total area of 1.555 km^2 on 2 September 2015, from TLS-derived high-resolution DEMs. Intensive glaciological investigations of UG1 were implemented in 1959 and then a monitoring station (Tien Shan Glaciological Station) was set up for long-term measurements. Over the past 50 years, UG1 had experienced two accelerated recessions, commencing in 1985 and 1996 respectively (Li et al., 2011). The glacier was separated into two branches in 1993 due to enhanced melting (Li et al., 2011).

UG1 is a typical summer-accumulation-type glacier in a continental climate setting. The westerly circulation is influenced by the dynamic action of the Tibetan Plateau in the summer months, causing a cold climate with little precipitation in the study site. During the summer month the Tibetan Plateau becomes a thermal depression and forms a plateau monsoon, which carries warm and humid air from the India Ocean, producing abundant precipitation surrounding the Plateau. These climatic conditions were confirmed by the annual climate records (1959-2015) of Daxigou Meteorological Station (DMS), located about 3 km southeast of UG1 at 3539 m a.s.l.; the annual average air temperature was about -5.0 ℃, and the annual average precipitation was 460 mm. 78% of the annual total precipitation amount occurs from May to August (summer), dominated by solid precipitation (Yue et al., 2017). The climatic

conditions mean that the glacier is dominated by weak accumulation from October to March (winter) and the accumulation rate is quicker from April to May; both strong ablation and accumulation mainly take place between June and September (Liu et al., 1997).

The mass balance of UG1 has been observed by measuring stakes or snow pits, beginning in 1959 (Xie and Liu, 2010). Glaciological measurements broke off during the period 1967-79 and the glaciological data series during this period were reconstructed from correlations with climatic data observed at the DMS. The program was re-established using glaciological methods in 1980.

3. Data and methodology

3.1. Terrestrial laser scanning

3.1.1. Principles and key features of Riegl VZ®-6000 TLS

Riegl VZ®-6000 TLS is an active laser imaging technique that calculates the distance between the object and the laser transmitter based on time-of-flight measurement with echo digitization and online waveform processing, and consequently the position of the point of interest to be computed (RIEGL Laser Measurement Systems, 2013). The scan mechanism includes a fast-rotating (60-120 ° from zenith) and more slowly rotating optical head (0-360 °). The mirror deflects the laser beam in different directions, thus forming a scan line from consecutive measurements. Meanwhile, the optical head rotates and this scan movement is called a frame scan. A line scan and frame scan generate a view scan using this technique; data collection occurs at a rate of 23 000-222 000 points per second and generates point clouds (Table 1; RIEGL Laser Measurement Systems, 2014a).

The high-accuracy and -precision ranging is based on its unique V-line technology of echo digitization and online waveform processing, which allows Riegl VZ®-6000 TLS to operate even in poor visibility and in demanding multi-target situations caused by dust, haze, rain, snow, etc. (RIEGL Laser Measurement Systems, 2014a).

3.1.2. Terrestrial laser scanning surveys

Multi-temporal terrestrial laser scanning data of UG1 were collected from four scan positions to achieve maximum coverage, and each scan location was selected from the directions where most glacier surface point clouds would be achieved (i.e. the best possible visibility to glacier surface terrain) (Fig. 1c, d). To avoid ground motion and to obtain accurate coordinates of point clouds, each scan position was fixed using reinforced concrete with a standard GPS-leveling point. 3-D coordinates of the four scan positions were then surveyed using the real-time kinematic (RTK) global positioning system (GPS, Unistrong E650 instrument) to facilitate the most accurate direct georeferencing and registration. The 3-D coordinates were acquired in the UTM 45N coordinate system in the WGS84 datum. The accuracy of this type of RTK surveys has been reported to be within ±1 cm horizontally and ±2 cm vertically, according to previous studies on UG1 (e.g. Wang et al., 2014; Wang et al., 2017).

After the measurements of 3-D coordinates, the Riegl VZ®-6000 was mounted on a tripod placed in the scan position to survey the glacier surface terrain. The scan parameters and atmospheric conditions are of crucial importance, directly determining point cloud data quality (point density and coverage) and acquisition time (Table 1). As to UG1, the laser pulse repetition rate was first set to 50 kHz, then line resolution and frame angle measurement resolution were set to 0.2 ° to allow a view scan with vertical and horizontal

angles in the range 60–120 ° from zenith and 0–360 °, respectively. A fine scan is a rectangular field-of-view scan, and the selected field should always cover the entire glacier to guarantee the overlap percentage of four scans was no less than 30% (CH/Z 3017-2015, 2015). With each scan, the laser pulse repetition rate was reset to 30 kHz, and the corresponding line and frame resolution were configured as 0.02 ° to ensure dense points of the glacier surface, except for the scan campaign on 2 September 2015 (Table 2). All scans are performed on sunny days (dry and windless atmosphere) to avoid the influence of precipitation and fog, which can absorb laser pulse and reduce the possible survey distance. Details of the survey parameters are listed in Table 2.

3.1.3. Terrestrial laser scanning data processing

Original point cloud data were post-processed with RiSCAN PRO® v 1.81 software; this includes direct georeferencing, data registration, vacuation and filtering (RIEGL Laser Measurement Systems, 2014b). For all five scan campaigns, four scan positions were used. In the first phase (i.e. direct georeferencing), the TLS data from the different scan positions had to be transformed from the Scanner's Own Coordinate System (SOCS) into a Global Coordinate System (GLCS). According to Figure 2, the transformation of a point from SOCS into the GLCS can be expressed by the vector equation

$$\overrightarrow{r_g} = \overrightarrow{r_0} + R(k)\overrightarrow{r_s}\,, \tag{1}$$

where $\overrightarrow{r_s}$ is the vector of a target in the SOCS; r_g is the vector of the georeferenced target in the GLCS; $\overrightarrow{r_0}$ is the vector of SOCS origin in the GLCS, k is the derived azimuth from the scan position to the backsight station and

$$R(k) = \begin{Bmatrix} \cos k & \sin k & 0 \\ \sin k & \cos k & 0 \\ 0 & 0 & 1 \end{Bmatrix}. \tag{2}$$

Hence the direct method of georeferencing uses the 3-D coordinates of the scan positions to realize its functions (Mukupa et al., 2016; Fey and Wichmann, 2017). The accuracy of the method depends on the quality of the measured coordinates. Previous studies stated that the direct georeferencing technique in TLS using global navigation satellite systems (GNSS) is advantageous (e.g. Mohamed and Wilkinson, 2009; Paffenholz et al., 2010).

The location of each scan was fixed in the GLCS after direct georeferencing; but the point clouds of the overlapped areas cannot coincide completely due to the influence of orientation. In the second step, multi-station adjustment (MSA) was used for the data registration of each scan position according to the iterative closest point (ICP) algorithm (Besl and McKay, 1992; Zhang, 1992). When we used MSA, the location of each scan was locked and the orientation of each scan was constantly adjusted in several iterations to compute the best overall fit for them based on least-squares minimization of residuals.

Afterwards we combined the overlapped scans in one layer. An octree algorithm was used to the merged layer to produce points with equal spacing to realize point cloud data vacuation (Schnabel and Klein, 2006; Perroy et al., 2010). A terrain filter was then applied to filter out noise and non-ground data due to atmospheric reflections such as dust or moisture, which still occurred despite scanning on fine days (RIEGL Laser Measurement Systems, 2014b). Visual interpretation was also performed to check the data and remove clear visual outliers. Finally, glacier surface point clouds with one layer were produced.

3.2. Geodetic mass balance

3.2.1. Geodetic mass balance calculations

As the orientation of each scan was continually adjusted to compute the best fit, the attitude angles of each scan campaign are different. Multi-temporal registration, also called relative registration, set the processed layer of 2 September 2015 as a reference;

alignment of other scan campaigns onto the reference layer was finished with ICP (MSA) algorithms to determine the spatial bias of the multi-temporal scans and extract accurate elevation changes (Revuelto et al., 2014; Gabbud et al., 2015). The relative registered layers were then exported into LAS data format for further processing. Multi-temporal registration of two consecutive campaigns is a crucial step and determines the reliability of TLS-derived surface elevation changes (Revuelto et al., 2014; López-Moreno et al., 2016; Fey and Wichmann, 2017).

After the relative registration procedure, interpolation of the processed point cloud data calculated high-resolution DEMs of the study site. The surface elevation change Δh_k at the individual pixel r was calculated by differencing the TLS-derived multi-temporal DEMs with ArcMAP 10.2 software. The total volume change ΔV was determined by summing the elevation change Δh_k of different time periods, and is expressed as

$$\Delta V = r^2 \sum_{k=1}^{K} \Delta h_k, \quad (3)$$

where K is the number of total pixels covering the maximum extent of UG1, and r is the pixel size (1 m × 1 m).

The calculated volume change is converted to geodetic mass balance (m w.e.) following:

$$B_{\text{geod}} = \frac{\Delta V}{\bar{S}} \cdot \frac{\rho}{\rho_{\text{water}}} = \frac{\Delta V}{1/2 \cdot (S_{t0} + S_{t1})} \cdot \frac{\rho}{\rho_{\text{water}}}, \quad (4)$$

where $\bar{S}$ is the mean glacier area of the two acquisition dates $t0$ and $t1$, thinking a linear change over time, ρ_{water} is the density of water and ρ is the average bulk density (density conversion) of glacier volume change (Thibert et al., 2008; Zemp et al., 2013).

3.2.2. Density conversion

As described above, the geodetic mass balance is calculated based on volume changes, which require a density conversion. However, the density is difficult to determine; in most studies, it is estimated and not measured. Some researches assume that no change occurs in the vertical firn density profile over time in the accumulation area and use glacier ice density for the conversion (Bader, 1954). Actually, the firn line, firn thickness and firn density all vary, and using the ice density causes an overestimate of mass balance. Huss (2013) recommended a density conversion of 850 ± 60 kg m^{-3} for the volume-to-mass conversion based on an empirical firn densification model with idealized surface mass balance forcing. But the recommendation is appropriate in the case of a geodetic observation span longer than 5 years; with stable mass balance gradients, volume changes are considerable and a firn area exists. Therefore, several recent studies classify the glacier surface into firn and bare-ice zones and use the volume-weighting method to calculate the annual conversion (e.g. Fischer et al., 2016; Klug et al., 2018). However, UG1 is a summer-accumulation-type glacier; mass balance processes primarily occur in summer and the glacier is dominated by weak accumulation in winter (Liu et al., 1997). Glacier volume changes in ice and firn usually occur at the same vertical profile according to long-term observations; the surface classification is not applicable in this study. Here we use in situ measured thickness and densities of firn/snow (ρ_{firn}) and ablation stake data (change in ice thickness) to calculate single-point density conversion:

$$\rho_i = \frac{\Delta h_{\text{ice}} \cdot \rho_{\text{ice}} + \Delta h_{\text{firn}} \cdot \rho_{\text{firn}}}{\Delta h_{\text{ice}} + \Delta h_{\text{firn}}}, \quad (5)$$

where ρ_{ice} = 900 kg m^{-3} is glacier ice density, and Δh_{ice} and Δh_{firn} are the changes in ice and firn/snow thickness, determined from glaciological measurements. We extrapolated single-point values to the glacier-wide densities to calculate average bulk density (ρ) using the interpolation method (Table 4), and the distributed density conversions of the total glacier were then generated (Fig. 6a, c, e, g).

It is generally true that the density conversion relies on measurements of changes in the 3-D firn body, thickness and density of each firn layer being continuous from the top to the bottom of the snow pit, and a stratigraphic description of the firn layers is completed by experienced investigators. Major change processes in the snowpack (e.g. from crystals to grains, free water content and ice layers, etc.) can be considered in this case (Kaser et al., 2003), and firn compaction assumed to be negligible. Glacier dynamics are probably insignificant for UG1 since the measured surface velocity is on the order of a few meters per year (Wang et al., 2017). Here we use the weighted average method (the weights are the thickness changes of each firn layer and glacier ice) to calculate the firn density (ρ_{firn}) of each snow pit.

3.3. Glaciological mass balance

3.3.1. In situ glaciological measurements of UG1

The mass-balance monitoring program of UG1 has been implemented by measuring stakes and snow pits (Xie and Liu, 1991). No less than 40 ablation stakes were drilled into the glacier evenly distributed at different elevation bands using a stream drill, despite the fact that the number of stakes has varied from year to year, and snow pits were dug where snow has accumulated (Fig. 1a). The mass-balance year of UG1 is defined from previous September 1 to next August 31 (Liu et al., 1997). Usually, from the beginning of May to early September each year, a spatial distribution of single-point ablation or accumulation, and snow density (if there is snow cover) were measured by stakes and snow pits at monthly intervals. Hence the measured items include the stake vertical height over the glacier surface, thickness of superimposed ice, and the thickness and density of each snow/firn layer at individual snow pits. Note that fresh snow covered the entire glacier at the beginning of the ablation season, so snow pits must also be dug at each of the stakes. The specific mass balance is calculated from the product of the level change between readings and the ice density. This study involves the glaciological measured data over the period 2015-17.

3.3.2 Glaciological surface mass-balance determination of UG1

Glaciological mass balance includes point and glacier-wide mass balances, and the point mass balance Δb over the time span from t_0 to t_1 is related to the mass-balance rate $\dot{b}$ (Cogley et al., 2011):

$$\Delta b = \int_{t_0}^{t_1} \dot{b}(t)\, dt = b(t_1) - \mathrm{b}(t_0). \quad (6)$$

Point values can be extrapolated to glacier-wide mass balance using the contour-line or profile method (Østrem and Brugman, 1991; Kaser et al., 2003). Here the time span is often a year or a season, and a seasonal mass balance is classically a winter balance or a summer balance (Cogley et al., 2011). Here t_0 and t_1 are the same as the t defined by Eq. (4). Point values can be extrapolated to glacier-wide specific mass balance using the contour-line or profile method (Østrem and Brugman, 1991; Kaser et al., 2003). For UG1, contour-line and isoline methods had successfully been used to calculate seasonal and annual glacier-wide mass balance, together with simulated values obtained using a simple energy-balance model in areas with no measurements (Xie and Liu, 1991; WGMS, 2017).

3.4. Glacier boundary delineation

Accurate glacier area was important for both geodetic and glaciological mass balance calculations (Zemp et al., 2013). Fresh snow cover probably led to an overestimate of glacier extent; to reduce the influence of snow cover and to extract accurate glacier outlines, we mainly considered glacier extents at the end of the ablation season. Glacier boundary delineation was performed following Abermann et al. (2010). Firstly three shade reliefs at the end of hydrological years 2015, 2016 and 2017 with an azimuth angle for illumination (300 °) were calculated based on multi-temporal high-resolution DEMs to show optimal visualization of contrasts in

different aspects. We then delineated the glacier boundary directly by manually digitizing the strongest roughness in the shade reliefs (Fig. 3). The area of UG1 was 1.555, 1.550 and 1.542 km^2 in 2015, 2016 and 2017 respectively. Glacier area reduction was primarily attributed to terminus retreat (Fig. 3b, c).

4. Uncertainty assessments

4.1. Uncertainties of geodetic mass balance

After multi-temporal registration, errors related to the spatial bias of the multi-temporal DEMs may be negligible. Besides density conversion for converting TLS-derived glacier surface elevation changes to mass balance, uncertainties in the geodetic mass balances derived from TLS may be related to (1) errors in point cloud data acquisition, including surface terrain and atmospheric conditions (moisture and wind) (Revuelto et al., 2014; Fischer et al., 2016); and (2) errors in data processing and DEM generation, e.g. registration (multi-station adjustment), point cloud vacuation and filtering (smoothing terrain information) (Wheaton et al., 2010; Gabbud et al., 2015; Hartzell et al., 2015).

As mentioned in Sect. 3.1.2, dry and windless days were selected to finish the five scan campaigns. Instability of the TLS influences the registration of single scan positions from each data acquisition campaign, which includes small displacements of scan positions and the vibration of TLS. Each scan position was stabilized on stable rock surfaces using reinforced concrete (the average drilling depth was greater than 80 cm) with a standardized GPS-leveling point to avoid ground motion. In fieldwork, TLS is mounted using a tribrach on a tripod to level the instrument (Xu et al., 2017). Revuelto et al. (2014) found that the vibration of TLS can introduce considerable errors in measurements performed over large scales. In our experience, this issue is mainly relevant to wind, so windless conditions are important. Because the registration error cannot be distinguished from the positional uncertainties and the surface, it is difficult to assess registration-induced uncertainty; the error statistics are usually used to evaluate the registration error (Fey and Wichmann, 2017). RiSCAN PRO® v 1.81 software reports error statistics of the MSA results (RIEGL Laser Measurement Systems, 2014b). The standard deviation of errors (σ_{MSA}) from the set of residuals obtained from registering the point cloud can be considered as an indication of registration quality (Gabbud et al., 2015; Fischer et al., 2016). σ_{MSA} values for the four periods over stable terrain surrounding UG1 are listed in Table 3. Registration quality was higher at seasonal than at annual scales; the higher quality may be attributable to fresh snow cover, which makes the stable terrain smooth.

Despite four scan positions placed at the terminus of UG1, two artefacts (two green polygons in Fig. 5) were due to flat terrain and relatively higher elevation of WB surface (Fig. 1a). We filled these regions using the spatial interpolation method, which can induce potential errors in DEM creations. The lack of dense measured 3-D coordinates of the terrain limits us to assessing terrain-induced errors quantitatively. Xu et al. (2017) compared the interpolated and measured surface elevation changes at corresponding ablation stakes and confirmed that the comparative results were encouraging. For precision, the artefacts were not taken into account in calculating the mass balance. Furthermore, supraglacial river developed widely at the strong ablation season due to glacier melting (Fig. 1c and d); its terrain characteristics are depicted by TLS. We observe the presence of outliers in these regions (Fig. 5). In order to preserve terrain information as much as possible, the octree algorithm built the topological relationship of scattered points to realize the vacuation of the point cloud. Point cloud filtering is also a significant post-processing step because of the dense ablation stake network, which is actually scanned by the device. Fortunately, fine scan generates high-density points of the glacier surface terrain.

The Cryosphere Discuss., https://doi.org/10.5194/tc-2018-128
Manuscript under review for journal The Cryosphere
Discussion started: 7 August 2018

There are no better ways to evaluate the uncertainty of DEMs without precise and well-distributed stable points (Bolch et al., 2017). The standard error ($\sigma_{\overline{\Delta h\mathrm{TLS}}}$) of elevation changes over stable terrain can be considered as a criterion of the uncertainty of the entire glacier (Rolstad et al., 2009; Zemp et al., 2013). The standard deviation ($\sigma_{\Delta h\mathrm{TLS}}$) of the stable terrain elevation changes is suitable for estimating the uncertainty of the DEM differences at the individual pixel scale (Fig. 4); in this case the standard error is defined as the standard deviation. However, the spatial auto-correlation must be considered when we calculate the uncertainty of the glacier-wide elevation changes. Thereby, the uncertainty of TLS-derived glacier-wide elevation changes ($\sigma_{\overline{\Delta h\mathrm{TLS}}}$) for individual glaciers were quantified using the geostatistical analysis methods of Rolstad et al. (2009) and written as

$$\sigma^2_{\overline{\Delta h\mathrm{TLS}}} = \sigma^2_{\Delta h\mathrm{TLS}} \cdot \frac{1}{5} \cdot \frac{S_{\mathrm{cor}}}{S}, \quad (7)$$

where $\sigma_{\Delta h\mathrm{TLS}}$ denotes the standard deviation of TLS-derived elevation changes over stable terrain. S_{cor} is spatially correlated area. Given the high density (> 1 point m^{-2}) of the TLS data, we can probably assume that the number of independent items is about the number of glacier pixels (cf. Joerg et al., 2012, ALS point clouds). Here we therefore assume $S_{\mathrm{cor}} = S$. This leads to calculated values of $\sigma_{\overline{\Delta h\mathrm{TLS}}}$ range from ±0.163 to ±0.250 m (Table 3).

Uncertainties related to the density conversion for a single point ($\sigma_{\rho i}$) were calculated as

$$\sigma_{\rho i} = \frac{\Delta h_{ice} \cdot \sigma_{\rho \mathrm{ice}} + \Delta h_{firn} \cdot \sigma_{\rho firn}}{\Delta h_{ice} + \Delta h_{firn}}, \quad (8)$$

where $\sigma_{\rho \mathrm{ice}}$ and σ_{firn} are uncertainties of ice and firn densities, which were assumed to be ±17 and ±50 kg m^{-3}, respectively, following Klug et al. (2018). We then extrapolated single-point values to glacier-wide uncertainties (σ_{ρ}) using the interpolation method on the ArcMAP 10.2 platform (Table 4). According to Huss et al. (2009), the uncertainties of the geodetic mass balance (σ_{geod}) can be estimated using

$$\sigma_{\mathrm{geod}} = \pm\sqrt{\left(\overline{\Delta h\mathrm{TLS}} \cdot \sigma_{\rho}\right)^2 + (\rho \cdot \sigma_{\overline{\Delta h\mathrm{TLS}}})^2}, \quad (9)$$

where $\overline{\Delta h\mathrm{TLS}}$ is the average of TLS-derived glacier-wide elevation changes and the related uncertainty relies on the accuracy of the used DEMs.

4.2. Uncertainties of glaciological measurements

Many difficulties, including the harsh climate, create problems and lead to additional sources of errors for glaciological measurements, which in turn cause uncertainties in glaciological mass balance that are not easy to quantify (Dyurgerov, 2002). Uncertainties in glaciological measurements were classified into three groups: (i) errors in field observations, (ii) errors related to spatial extrapolation over the entire glacier and (iii) errors due to non-updated glacier area. Note that the class (iii) uncertainties appeared to be negligible due to the short time intervals (two consecutive years) in our study.

Point measurement uncertainties are prone to errors in stake readings and snow/firn density measurements (Jansson and Pettersson, 2007; Thibert et al., 2008; Huss et al., 2009), sinking or melting-out of stakes and misidentification of the firn layer surface at the end of the last hydrological year (Zemp et al., 2010). Some studies have demonstrated errors of ±0.1 and ±0.3 m w.e. for reading stakes in the ablation and accumulation areas, respectively (Huss et al., 2009). Zemp et al. (2010) determined an overall stochastic uncertainty at ±0.2 m w.e. a^{-1} for field measurements. Zemp et al. (2013) reanalyzed the mass balance of Hintereisferner, Austria, from 1953 to 2006 (six time intervals) and found an uncertainty of ±0.2 m w.e. a^{-1}. Beedle et al. (2014) suggested an error of ±0.1 m w.e. a^{-1} for accumulation-area measurements. For Nigardsbreen (Norway) glaciers, Andreassen et al. (2016) calculated a point

measurement of ±0.21 m w.e. a^{-1} by summing false determination of the summer surface (±0.2 m w.e. a^{-1}), subsidence of stakes (0.20 m w.e. a^{-1}) and errors in density measurements (0.05 m w.e. a^{-1}). Following Thibert et al. (2008), here errors of ablation measured in ice (σ_a^{ice}) and firn (σ_a^{firn}) are calculated using $0.14/\sqrt{N_a^{ice}}$ and $0.27/\sqrt{N_a^{firn}}$, respectively, where N_a^{ice} and N_a^{firn} denote the number of sampling sites, respectively; errors in accumulation measurements (σ_c) are determined based on $0.21/\sqrt{N_c}$, where N_c is the number of snow pits.

The class (ii) errors originate from extrapolating observed values to unmeasured areas, insufficient spatial distribution of measured sites and the interpolation method. Hock and Jensen (1999) evaluated the error of the interpolation method at about ±0.1 m w.e. a^{-1} for mean specific mass balances. Huss et al. (2009) computed and compared mean specific net balance with randomly reduced annual stake datasets and found that the error was ±0.12 m w.e. a^{-1}. For UG1, the firn basin and glacier tongue terrain of the WB are very steep and the upper eastern elevation of the EB is also precipitous, resulting in no in situ measurements are available in theses inaccessible areas. Here we mainly consider errors in the unmeasured areas and conservatively assume that the corresponding uncertainty σ_{extra} was ±0.1 m w.e. a^{-1} (cf. Andreassen et al., 2016).

Taking into account the above-mentioned factors, the uncertainty of the glaciological mass balance σ_{glac} is calculated as (Table 4)

$$\sigma_{glac} = \sqrt{(\sigma_a^{ice})^2 + (\sigma_a^{firn})^2 + \sigma_c^2 + \sigma_{extra}^2} \quad . \tag{10}$$

5. Results

5.1. Spatial patterns in TLS-derived surface elevation changes

The high-accuracy and -resolution DEMs allowed a detailed insight into the glacier surface elevation changes. TLS-derived distributed elevation changes of both branches are generally similar in their spatial patterns. Strong mass losses visibly occurred across the ablation area, with smaller lowering to slight thickening in the upper-elevation parts (Fig. 5a, c, e); this altitudinal changing pattern is in good agreement with the long-term glaciological measurements. But in the mass-balance year 2016-17, the altitudinal changing pattern of WB was not pronounced (Fig. 5g). Compared to the mass-balance year 2015-16, areas of clear increase were observed in the upper eastern parts of EB in the second mass-balance year. In addition, ice losses in the lower parts of WB and glacier thickening in the upper reaches of WB were greater and surface lowering of EB was more pronounced near the glacier tongue (Fig. 5g). During summer 2015, surface lowering mainly occurred in the ablation areas of EB (Fig. 5a). Glacier surface elevation changes were significantly more negative in summer 2016 than in the first summer; clear surface lowering of EB was observed (Fig. 5e). There are some curves of pronounced surface lowering in the ablation areas, especially in summer, which are related to supraglacial river (Fig. 1c, d). In addition, a slight thinning area is detected at the lower (northerly) edge of EB, which may be associated with debris cover (Fig. 1c).

5.2. Glacier-wide elevation and geodetic mass changes

TLS-derived glacier-wide mass balances (Table 4) and their spatial distributions (Fig. 6b, d, f, h) were calculated by multiplying the spatially distributed glacier surface elevation changes (Fig. 5a, c, e, g) by the corresponding distributed density conversion (Fig. 6b, d, f, h). The annual density conversions were generally higher than the summer ones (Table 4), because the thicker snow and firn covered most parts of the glacier surface at the beginning of the hydrological year, and the ablation area was bare ice or covered a thin snow at the end of the ablation season. Thus the summer geodetic mass balance was highly affected by the snow and firn, and

the magnitude of the altitudinal variability in the summer mass balance significantly changed when compared to elevation changes (Fig. 5a, c), whereas the spatial distributed patterns between elevation changes and mass balances showed good performances. These suggest that the density conversions vary for all of the studied periods and a constant value used as the conversion is clearly inappropriate. Here in situ measured densities from snow pits improved the accuracy of TLS-derived geodetic mass-balance calculations and therefore provided exceptional level of detail on glacier-wide mass balance.

UG1 experienced negative surface elevation changes and mass balances for all four investigated periods (Table 4). Summer elevation lowering and mass loss were slightly greater than annual decreases, which may be related to the climatic conditions observed at DMS (see Sect. 2). In the mass-balance year 2015-16, calculated glacier-wide geodetic mass balance was -0.722 ±0.186 m w.e., which was slightly more negative than in the second mass-balance year. Summer and annual mass balances of WB were more negative, except for summer 2016 when the mass loss of EB was greatest.

5.3. Comparison to in situ glaciological measurements

TLS-derived geodetic elevation changes at individual stakes closely matched the glaciological elevation change (changes in stake height) of individual stakes from in situ measurements (Fig. 5). The correlation coefficients (R^2) between the glaciological elevation change at the ablation stakes and TLS-derived geodetic elevation change at corresponding points were more than 0.90 (Fig. 7). Note that the locations and number of the sites varied slightly over time due to stake melt-out, in order to objectively assess the accuracy of the geodetic elevation changes, we selected the best-monitored glaciological single-point results. The majority of the point elevation changes from TLS measurements were slightly positive compared to the glaciological ones, except for summer 2016. During summer 2016 and mass-balance years 2015-16 and 2016-17, the mean values of Δh_{TLS} - Δh_{glac} were 0.18, 0.25 and 0.14 m, respectively, which is systematically less than the corresponding uncertainties ($\sigma_{\overline{\Delta h \mathrm{TLS}}}$) of the glacier-wide elevation differences. Considering that the glacier dynamic thickening and thinning were tiny since the observed vertical ice velocity was small (cf. Beedle et al., 2014), the TLS-derived surface-elevation changes captured most of the major changing patterns from the glaciological measurements.

The varying tendencies of the glaciological mass balances coincided with the geodetic ones (Table 4). In 2016-17, the difference ($\Delta B = B_{\mathrm{glac}} - B_{\mathrm{geod}}$) in glacier-wide mass balances of UG1 between the two methods was close to zero (ΔB = -0.006 m w.e.). Remarkable differences were detected in summer 2015 for UG1 and EB, with ΔB = -0.240 m w.e. and ΔB = -0.269 m w.e., respectively. In other three periods, the differences between the two methods were much less the uncertainties of ΔB, which were calculated based on the law of error propagation ($\pm\sqrt{\sigma_{\mathrm{geod}}^2 + \sigma_{\mathrm{glac}}^2}$). Overall, the differences of UG1 were slightly smaller than those of the two branches (Fig. 7). In order to calculate the statistical significance between the two methods and validate the geodetic against the glaciological mass balance, the reduced discrepancy (δ) between the two methods was calculated following Zemp et al. (2013, Eqs. 19-21); the results of δ range from -1.143 to 0.579. As δ falls within the 95% ($|\delta| < 1.96$) and 90% ($|\delta| < 1.64$) confidence interval, good agreement between the glaciological and geodetic methods can be considered as satisfying.

The mass balance elevation distribution derived from the two methods remained similar despite the presence of differences in magnitude, i.e. mass balance increased with rising altitude (Fig. 8). The geodetic results were more positive in lower-elevation regions and more negative in the higher glacier parts in general; this phenomenon was probably related to glacier dynamics. The

dotted (glaciological) and solid (geodetic) lines met where the glacier mass balances were close to zero; this meant that the equilibrium-line altitudes (ELAs) derived from the two methods matched closely, especially in mass-balance year 2015-16 and summer 2016 (Fig. 7), but the biggest shift between the two methods was detected in summer 2015 for EB, which may be related to the reasons mentioned in Sect. 6.3. This reflects that the TLS can be therefore considered as an effective tool to calculate ELA.

6. Discussion

6.1. The quality of point cloud data and DEM differencing

The important factors for scanning high-quality point cloud data are visual angles of the scan positions and atmospheric conditions. A dry and windless atmosphere is a prerequisite for high-quality data acquisition. Good visual angles can easily be achieved for very small cirque glaciers. Generally, the area and length of reference glaciers are greater, with a huge variation in altitude. The maximum working distance (6 km) of Riegl VZ®-6000 is specified for flat targets with size in excess of the laser beam diameter, perpendicular angle of incidence, and atmospheric visibility in excess of 23 km. In bright sunlight the operational range may be considerably shorter than under an overcast sky (Table 1; RIEGL Laser Measurement Systems, 2014a). However, glaciers generally have complicated surface terrain and the requirement of perpendicular angle of incidence is not always met, so the unscanned regions usually have flatness or alcove terrains (Fig. 4). It is very difficult for us to get a dry and windless atmosphere under an overcast sky around a glacier. In these situations, more than one scan position must be set in order to scan as much of the glacier surface area as possible. However, this, in turn, can create errors in data registration. The average error originating in MSA (σ_{MSA}) of the investigated periods was ±0.153 m (Table 3). Actually, σ_{MSA} is highly dependent on the overlap percentage of point clouds from each scan position of the same survey data and the accuracy of global 3-D coordinates of each scan position. In our fieldwork, the overlap percentage of point clouds from the four scan positions was more than 30%, which met the requirements of data registration (CH/Z 3017-2015, 2015). Note that we do not found that the more scan positions the better since more scan positions will probably decrease the quality of MSA. We should find the best visual angles to obtain the maximum scan range with the fewest scan positions. Higher elevation favors better angles, but it is not always easy for us to access higher parts and place the instrument. For the ideal distribution, scan positions should locate in different elevation bands and directions (Fig. 1a). In addition we can also mount a steadying bar on a tripod to raise the altitude of the TLS.

Systematic shifts of DEMs in the horizontal and vertical directions can also increase the uncertainty of DEM differencing (Nuth and Kääb, 2011), so multi-temporal registration of two consecutive scan campaigns is predicated on the TLS-derived geodetic elevation changes being accurate. The mean uncertainty of elevation changes was ±0.215 m (Table 3), which was slightly smaller than in the TLS datasets used for other glacier thinning measurements (e.g. López-Moreno et al., 2016). This may be attributable to the use of accurate global 3-D coordinates of scan positions and a sufficient number of stable terrains (Fig. 3). In addition, fixed scan positions also reduce multi-temporal registration error and enhance the accuracy of glacier-wide elevation changes. So the quality of point cloud data and DEM differencing are encouraging.

6.2. Geodetic and glaciological mass balances

It is obvious that the quality of TLS-derived geodetic mass balances relies on the accuracy of glacier surface elevation changes and density conversion of volume to mass changes. With regard to density conversion, our approaches account for the 3-D changes of ice and firn/snow bodies as well as the corresponding densities to calculate more accurate values of density (Table 4). The annual ρ

The Cryosphere Discuss., https://doi.org/10.5194/tc-2018-128
Manuscript under review for journal The Cryosphere
Discussion started: 7 August 2018

values were in the range of 763-865 kg m^{-3}, which is in line with the average density of 850 ± 60 kg m^{-3} recommended by Huss (2013), whereas, ρ of WB declined to 763 kg m^{-3} in the mass-balance year 2015-16, largely because of the presence of fresh snow cover at the time of the glaciological measurements (see Sect. 6.3). For the same reason, the summer values concurred with the recommended density. Calculated uncertainties in the geodetic mass balances ranged from ±0.132 to ±0.197 m w.e., with an average value of ±0.164 m w.e. for the investigated periods (Table 4) and were slightly greater than other geodetic mass balance measured base on the same TLS device (e.g. Fischer et al., 2016), which may be related to multiple scan positions and a larger scanning range, but smaller than those derived from remote sensing imagery (e.g. Holzer et al., 2015; Barandun et al., 2018).

Dense spatially measured sites cover the glacier surface (the average density is about 28 stakes km^{-2}), except for the inaccessible areas (Fig. 1a), to measure the glaciological mass balance. The mean uncertainty of σ_{glac} was ±0.115 m w.e., mainly originating from spatial extrapolation. This value is smaller than in most recent studies (e.g. Andreassen et al., 2016; Thomson et al., 2017; Klug et al., 2018). This is probably due to relative smaller area and accompanying higher density of point measurements of UG1 than aforementioned glaciers (Fig. 1a).

Thus the TLS device yields accurate geodetic results and the quality of the glaciological mass balances is also very good. Nonetheless, the glaciological method cannot measure internal and basal mass balances, but these processes are implicitly captured by the repeated geodetic surveys. We need to provide a rough estimate of internal and basal mass balances of UG1 to detect their contributions to the differences between glaciological and geodetic mass balances. UG1 is a cold glacier, and its internal ablation (B_{pe}) is weak (Huang, 1999; Albrecht et al., 2000), mainly because of the released potential energy of descending water:

$$B_{pe} = \frac{Q_m g}{L_f \bar{s}} \cdot \frac{\bar{h}_{ELA} - h_{term}}{2}, \quad (11)$$

where Q_m = 1.8×10^6 m^3 a^{-1} denotes annual discharge of flowing water, g is the gravitational acceleration, and $\bar{h}_{ELA}$ and h_{term} are ELA and the altitude of the glacier terminus, respectively. Basal ablation from geothermal heating (B_{gt}) was evaluated using

$$B_{gt} = \frac{qt}{L_f \rho_{water}}, \quad (12)$$

where q = 0.059 W m^{-2} is the geothermal heat flux (Huang, 1999), L_f is the latent heat of fusion and t is the mass-balance period; here we primarily consider annual scale. Finally, the calculated internal and basal ablation totaled -0.006 m w.e. a^{-1}.

We assessed internal accumulation dominated by refreezing percolating water in the cold interior of the glacier as well as the freezing of water in cold snow and firn following Zemp et al. (2010), who assumed that internal accumulation was 4% of the winter mass balance, and the resulting value was about 0.01 m w.e. a^{-1} in this study. Finally we estimated the total value for internal and basal mass balances at 0.004 m w.e. a^{-1}, which is far less than the difference (ΔB) between the two methods. This suggests that the contribution of annual internal and basal processes is negligible and does not affect the differences between the two methods.

6.3. Meteorological and glacier surface terrain considerations

Glacier mass balance is the direct and undelayed respond to meteorological conditions (Zemp et al., 2009). Figure 9 shows daily meteorological records provided by DMS from 25 April 2015 to 28 August 2017. Positive temperature and more than 75% of the annual total precipitation amount occurred simultaneously during the summer months; this probably resulted in summer mass balances that were slightly more negative than annual ones (Table 4). Although the observed discrepancies are relatively small, the above-mentioned differences in summer 2015 had not been statistically identified. One possible reason is the presence of fresh snow cover at the time of TLS surveys according to field observation. The glaciological measurements of EB were performed five days before the TLS surveys (28 August-2 September 2015). The total precipitation was 67 mm and daily mean temperatures were close

to zero (Fig. 9), besides the daily minimum temperatures were all below 0 ℃ during the five days. The climatic conditions may be responsible for the larger mass-balance differences of EB. In addition, light snow occurred on the eve of the latest TLS surveys (28 August 2017), possibly resulting in the noticeable increase in the upper eastern parts of EB (Fig. 6h).

The differences in mass balance between the two methods were possibly related to the effect of glacier surface terrain. The presence of two minimal artefacts in TLS surveys is due to the flat terrain of WB surface (two green polygons in Fig. 5). The geodetic mass-balance calculations did not include these artefacts; this cloud potentially increased the difference between the two methods. Furthermore, these undetected regions located in the ablation area and higher wastage than the surroundings were observed according to glaciological measurements. This may imply that the geodetic mass balances of WB were more positive than the glaciological ones (Table 4) and a discrepancy in mass balance elevation distributions of WB at 4000-4150 m a.s.l. Nevertheless, the geodetic method is able to cover the majority of the glacier surface and takes the terrain characteristics into account, whereas the glaciological measurements cannot capture all the topographic features despite a dense spatial coverage of in situ observations being applied, and what's more, in situ observations are missing in the firn basin and glacier tongue terrain of WB and eastern elevations of EB because of the presence of precipitous terrains in these inaccessible regions (green color in Fig. 10a). The eastern elevations of EB were dominated by the northwest aspect, and the firn basin had aspects from north to northwest (Fig. 10b), aspects that were likely to influence the glacier surface albedo and thereby control the surface change patterns (cf. Yue et al., 2017).

6.4. Potential of the long-range TLS applied in glacier mass balance monitoring

This study presents the application of multi-temporal Riegl VZ®-6000 TLS point clouds in mass balance monitoring of UG1. The long-range TLS can provide high-temporal-spatial-resolution and -accuracy DEMs to allow more detailed insight into glacier evolution (e.g. Gabbud et al., 2015; Fischer et al., 2016). To take advantage of this and provide more-precise glacier surface elevation changes, it is worth remembering that fixed scan positions are highly important between consecutive scans when using our approach. We should also note that not all glaciers in China are as easily accessible as UG1. For many large glaciers, it is not always easy to fix scan positions using reinforced concrete with a standard GPS-leveling point, but we can mark stable bedrock outcrop as a scan site. Another advantage of this type of TLS is the long scanning range, and such an instrument could allow most of the glacier surface to be scanned from one or several scan positions, especially for remote and inaccessible glacier areas (e.g. crevasses, steep ice, debris cover, etc.). Therefore the instrument provides a quantitative evolution in spatial coverage compared to glaciological in situ measurements, which can be seen as a beneficial complement to glaciological mass balance, particularly for calibrating inaccessible areas. TLS surveys can provide updated glacier boundary and surface DEMs, and the location of stakes may also be identified based on high-quality point clouds; all of these parameters are favorable for glaciological mass-balance calculations. A combination of glaciological and TLS observations may yield optimum results. Besides, TLS-derived geodetic results can validate the distributed glacier mass-balance models.

Now the TLS has been successfully applied to monitor mass balance of UG1. From our experience, the monitoring tool is potentially applicable to other glaciers provided that these glaciers have small to medium size and relative steep terrain. According to the second Chinese glacier inventory (CGI-2), most glaciers (~83% of the total number) in western China have an area smaller than1 km^2 and only ~3% of glaciers have an area lager than 5 km^2, and the mean glacier surface slope of GIC-2 is 19.9 °(Guo et al., 2015), which is very close to corresponding value of UG1 (23.4 °) (Fig. 10a). Therefore, the majority of glaciers can be measured using the TLS. Furthermore, if we assume that glaciers with an area of ≤ 1.555 km^2 (area of UG1) and a surface slope greater than

23.4 ° have a good visibility to be monitored using the TLS, the number of appropriate glaciers is ~58.5% of the total. So the TLS system has huge application potential for glacier mass-balance monitoring in China.

Nevertheless, note that we use the in situ measured densities of UG1 to calculate density conversion, which requires extensive field observations. Density conversion over short time periods and point cloud data post-processing are challenges that need to be met for a broader application of the long-range TLS. TLS requires specific knowledge, skills and experience for its use and data processing. The limitations of this TLS are related to suitable scan positions for obtaining good visual angles of the glacier surface and stable scan positions for multi-temporal registration of repeated scans for change detection. For density, we may consider using unmanned aerial systems and microwave remote sensing to measure snow depth and density of remotely located glaciers in future studies (see e.g. Bühler et al., 2016; Lemmetyinen et al., 2016). For longer time intervals (≥ 5 years), a density assumption based on physical models is also important since most glaciers in northwest China are cold and multi-thermal.

7. Conclusions

UG1 is one of the reference glaciers in the WGMS network, a representative glacier in Central Asia and the best-monitored glacier in China. Here, for the first time, we have presented the potential of a novel long-range TLS to monitor summer and annual geodetic mass balances of UG1. The Riegl VZ®-6000 TLS has long scan range up to 6 km and is exceptionally well suited for measuring snowy and icy terrains in glacier mapping. We use TLS-derived DEMs to calculate summer and annual surface elevation changes and geodetic mass balances of the glacier for two consecutive years (2015-17) as well as to delineate accurate glacier boundaries.

Our analysis suggests that UG1 has experienced pronounced thinning and mass loss for the four investigated periods. Glacier surface elevation lowering and mass loss during the summer were slightly greater than annual values. Glacier-wide geodetic mass balance in the mass-balance year 2015-16 was -0.722 ± 0.186 m w.e., which is slightly more negative than in the second mass-balance year. The majority of TLS-derived geodetic elevation changes at individual stakes were slightly positive, but insignificant compared to the glaciological elevation change (changes in exposed stake height) of individual stakes ($R^2 \geq 0.90$). The difference in glacier-wide mass balances of UG1 between the two methods was close to zero in 2016-17 but relatively larger differences were detected in summer 2015 for UG1 and EB, which were related to the presence of fresh snow at the time of TLS surveys. Statistical analysis shows that agreement between the glaciological and geodetic methods can be considered as satisfying.

Despite uncertainties inherent in TLS-derived geodetic mass balances, our results show that the TLS device yields reliable results and is therefore well suited to the study of reference glaciers such as UG1, which provide accurate and detailed information on glacier area and mass balance changes. Its temporal-spatial resolution allows more detailed insight into the glacier's evolution. The greatest strength of the TLS is the long-range scanning which allows most of the glacier surface to be measured, including areas that are inaccessible for in situ measurements. Use of the TLS-based geodetic method will be an important development since it is clearly a beneficial complement to direct glaciological mass balance, particularly for calibrating the unmeasured areas. A combination of glaciological and TLS observations may yield the optimum results. For a broader application of the long-range TLS, we should consider the quality of point cloud and DEM differencing and density conversion over short time periods.

Data availability. Glaciological mass balance data related to this study are submitted to the WGMS and will be available at website: http://wgms.ch/. TLS point cloud data are available upon request by email to the corresponding author.

Competing interests. The authors declare that no competing interests are present.

Acknowledgements. This work was supported by the National Natural Science Foundation of China (41471058, 91425303, 41721091and 41771081), State Key Laboratory of Cryospheric Science (SKLCS-ZZ-2018), Key Research Program of Frontier Sciences of Chinese Academy of Sciences (No. QYZDB-SSW-SYS024) and the West Light Program for Talent Cultivation of Chinese Academy of Sciences. We thank the Tien Shan Glaciological Station for the continuous field observations.

References

Abermann, J., Fischer, A., Lambrecht, A., and Geist, T.: On the potential of very high-resolution repeat dems in glacial and periglacial environments, The Cryosphere, 4, 53-65, https://doi.org/10.5194/tc-4-53-2010, 2010.

Albrecht, O., Jansson, P., and Blatter, H.: Modelling glacier response to measured mass-balance forcing, Ann. Glaciol., 31, 91– 96, 2000.

Andreassen, L. M., Elvehøy, H., Kjøllmoen, B., and Engeset, R. V.: Reanalysis of long-term series of glaciological and geodetic mass balance for 10 Norwegian glaciers, The Cryosphere, 10, 535–552, https://doi.org/10.5194/tc-10-535-2016, 2016.

Bader, H.: Sorge's law of densification of snow on high polar glaciers, J. Glaciol., 2, 319–323, 1954.

Barandun, M., Huss, M., Usubaliev, R., Azisov, E., Berthier, E., Kääb, A., Bolch, T., and Hoelzle, M.: Multi-decadal mass balance series of three Kyrgyz glaciers inferred from modelling constrained with repeated snow line observations, The Cryosphere, 12, 1899–1919, https://doi.org/10.5194/tc-12-1899-2018, 2018.

Beedle, M. J., Menounos, B., and Wheate, R.: An evaluation of mass-balance methods applied to Castle creek Glacier, British Columbia, Canada, J. Glaciol., 60, 262–276, https://doi.org/10.3189/2014JoG13J091, 2014.

Besl, P. and McKay, N.: A method for registration of 3-D shapes. IEEE Transactions on Pattern Analysis and Machine Intelligence, 14, 239–256, 1992.

Bolch, T., Pieczonka, T., Mukherjee, K., and Shea, J.: Brief communication: Glaciers in the Hunza catchment (Karakoram) have been nearly in balance since the 1970s, The Cryosphere, 11, 531–539, https://doi.org/10.5194/tc-11-531-2017, 2017.

Bühler, Y., Adams, M. S., Bösch, R., and Stoffel, A.: Mapping snow depth in alpine terrain with unmanned aerial systems (UAS): potential and limitations, The Cryosphere, 10, 1075–1088, http://dx.doi.org/10.5194/tc-10-1075-2016, 2016.

CH/Z 3017-2015.: Technical specifications for three-dimensional laser scanning. Beijing: National Administration of Surveying, Mapping and Geo-information of the People's Republic of China, p. 17, 2015.

Chen, Y., Li, W., Deng, H., Fang, G., and Li Z.: Changes in Central Asia's Water Tower: Past, Present and Future, Sci. Rep., 6, 35458, https://doi.org/10.1038/srep35458, 2016.

Cogley, J. G.: Geodetic and direct mass balance measurements: Comparison and joint analysis, Ann. Glaciol., 50, 96–100, https://doi.org/10.3189/172756409787769744, 2009.

Cogley, J. G., Hock, R., Rasmussen, L. A., Arendt, A. A., Bauder, A., Braithwaite, R. J., Jansson, P., Kaser, G., Möller, M., Nicholson, L., and Zemp, M.: Glossary of Glacier Mass Balance and Related Terms, IHP-VII Technical Documents in Hydrology No. 86, IACS Contribution No. 2, UNESCO-IHP, Paris, 2011.

Cox, L. H. and March, R. S.: Comparison of geodetic and glaciological mass balance, Gulkana Glacier, Alaska, USA, J. Glaciol., 50, 363–370, https://doi.org/10.3189/172756504781829855, 2004.

Cuffey, K. M. and Paterson, W. S. B.: The Physics of Glaciers, El-sevier, Amsterdam, 4 edn., 2010.

Dyurgerov, M. B.: Glacier mass balance and regime: data of measurements and analysis, Occasional Paper No. 55, Boulder, Colorado, available at: http://instaar.colorado.edu/other/occ papers. html, access: 12 March 2011, 2002.

Farinotti, D., Longuevergne, L., Moholdt, G., Duethmann, D., Mölg, T., Bolch, T., Vorogushyn, S., and Güntner, A.: Substantial glacier mass loss in the Tien Shan over the past 50 years, Nature Geosci., 8, 716–723, https://doi.org/10.1038/NGEO2513, 2015.

Fey, C. and Wichmann, V.: Long-range terrestrial laser scanning for geomorphological change detection in alpine terrain – handling uncertainties, Earth Surf. Process, Landforms, 42, 789–802, https://doi.org/10.1002/esp.4022, 2017.

Fischer, A.: Comparison of direct and geodetic mass balances on a multi-annual time scale, The Cryosphere, 5, 107–124, https://doi.org/10.5194/tc-5-107-2011, 2011.

Fischer, M., Huss, M., Kummert, M., and Hoelzle, M.: Application and validation of long-range terrestrial laser scanning to Monitor the Mass Balance of very small Glaciers in the Swiss Alps, The Cryosphere, 2016, 10, 1279–1295, http://dx.doi.org/10.5194/tc-10-1279-2016, 2016.

Gabbud, C., Micheletti, N., and Lane, S. N.: Lidar measurement of surface melt for a temperate Alpine glacier at the seasonal and hourly scales, J. Glaciol., 61, 963–974, http://dx.doi.org/10.3189/2015JoG14J226, 2015.

Guo, W., Liu, S., Xu, J., Wu, L., Shangguan, D., Yao, X., Wei, J., Bao, W., Yu, P., Liu, Q., and Jiang, Z.: The second Chinese glacier inventory: data, methods and results, J. Glaciol., 61, 357– 372, http://dx.doi.org/10.3189/2015JoG14J209, 2015.

Hartzell, P. J., Gadomski, P. J., Glennie, C. L., Finnegan, D. C., and Deems, J. S.: Rigorous error propagation for terrestrial laser scanning with application to snow volume uncertainty, J. Glaciol., 61, 1147–1158, http://dx.doi.org/10.3189/2015JoG15J031, 2015.

Haeberli, W., Hoelzle, M., Paul, F., and Zemp, M.: Integrated monitoring of mountain glaciers as key indicators of global climate change: the european alps, Ann. Glaciol., 46, 150-160, http://dx.doi.org/10.3189/172756407782871512 , 2007.

Hock, R., and Jensen, H.: Application of kriging interpolation for glacier mass balance computations, Geogr. Ann. A., 81, 611–619. http://dx.doi.org/10.1111/1468-0459.00089, 1999.

Hoelzle, M., Azisov, E., Barandun., Huss, M., Farinotti, D., Gafurov, A., Hagg, W., Kenzhebaev, R., Kronenberg, M., Machguth, H., Merkushkin, A., Moldobekov, B., Petrov, M., Saks, T., Salzmann, N., Schöne, T., Tarasov, Y., Usub-aliev, R., Vorogushyn, S., Yakovlev, A., and Zemp, M.: Re-establishing glacier monitoring in Kyrgyzstan and Uzbekistan, Central Asia, Geosci. Instrum. Method. Data Syst., 6, 397-418, https://doi.org/10.5194/gi-6-397-2017, 2017.

Holzer, N., Vijay, S., Yao, T., Xu, B., Buchroithner, M., and Bolch, T.: Four decades of glacier variations at Muztagh Ata (eastern Pamir): a multi-sensor study including Hexagon KH-9 and Pléades data, The Cryosphere, 9, 2071–2088, https://doi.org/10.5194/tc-9- 2071-2015, 2015.

Huang, M.: Forty year's study of glacier temperature in China. J. Glaciol. Geocryol. 21, 193–199, 1999, (in Chinese with English summary).

Huss, M., Bauder, A., and Funk, M.: Homogenization of long-term mass balance time series, Ann. Glaciol., 50, 198–206, https://doi.org/10.3189/172756409787769627, 2009.

Huss, M.: Density assumptions for converting geodetic glacier volume change to mass change, The Cryosphere, 7, 877–887, https://doi.org/10.5194/tc-7-877-2013, 2013.

Jansson, P. and Pettersson, P.: Spatial and temporal characteristics of a long mass balance record, Storglaciären, Sweden, Arct. Antarct. Alp. Res., 39, 432–437, 2007.

Joerg, P. C., Morsdorf, F., and Zemp, M.: Uncertainty assessment of multi-temporal airborne laser scanning data: A case study on an Alpine glacier, Remote Sens. Environ., 127, 118–129, https://doi.org/10.1016/j.rse.2012.08.012, 2012.

Kaser, G., Fountain, A., and Jansson, P.: A manual for monitoring the mass balance of mountain glaciers, IHP-VI Technical documents in Hydrology, p. 135, 2003.

Kaser, G., Cogley, J.G., Dyurgerov, M.B., Meier, M.F., and Ohmura, A.: Mass balance of glaciers and ice caps: consensus estimates for 1961–2004. Geophys. Res. Lett., 33, L19501, http://dx.doi.org/10.1029/2006GL027511, 2006.

Kerr, T., Owens, I., Rack, W., and Gardner, R.: Using ground-based laser scanning to monitor surface change on the rolleston glacier, New Zealand, J. Hydrol. (NZ)., 48(2), 59-72, 2009.

Klug, C., Bollmann, E., Galos, S. P., Nicholson, L., Prinz, R., Rieg, L., Sailer, R., Stötter, J., and Kaser, G.: Geodetic reanalysis of annual glaciological mass balances (2001–2011) of hintereisferner, Austria, The Cryosphere, 12, 833-849, https://doi.org/10.5194/tc-12-833-2018, 2018.

Lemmetyinen, J., Schwank, M., Rautiainen, K., Kontu, A., Parkkinen, T., Mätzler, C., Wiesmann, A., Wegmüller, U., Derksen, C., Toose, P., Roy, A., and Pulliainen, J.: Snow density and ground permittivity retrieved from L-Band radiometry: application to experimental data, Remote Sens. Environ., http://dx.doi.org/10.1016/j.rse.2016.02.002, 2016.

Li, J., Li, Z., Zhu, J., Li, X., Xu, B., Wang, Q., Huang, C., and Hu, J.: Early 21st century glacier thickness changes in the Central Tien Shan. Remote Sens. Environ., 192, 12-29, https://doi.org/10.1016/j.rse.2017.02.003, 2018.

Li, Z., Li, H., and Chen Y.: Mechanisms and simulation of accelerated shrinkage of continental glaciers: a case study of Urumqi Glacier No. 1 in Eastern Tianshan, central Asia. J. Earth Sci., 22, 423–430. http://dx.doi.org/10.1007/s12583-011-0194-5, 2011.

Lichti, D.D., Gordon, S. J., Tipdecho, T.: Error models and propagation in directly georeferenced terrestrial laser scanner networks, J. Surv. Eng., 131, 135–142. http://dx.doi.org/10.1061/ (ASCE) 0733-9453(2005)131:4(135), 2005.

Ligtenberg, S. R. M., Helsen, M. M., and van den Broeke, M. R.: An improved semi-empirical model for the densification of Antarctic firn, The Cryosphere, 5, 809–819, https://doi.org/10.5194/tc-5-809-2011, 2011.

Liu, C., Xie, Z., and Wang, C.: A research on the mass balance process of Glacier No.1 at the headwaters of the Urumqi River, Tianshan Mountains, J. Glaciol. Geocryol., 19, 17–24, 1997, (in Chinese with English summary).

Liu, Q. and Liu, S.: Response of glacier mass balance to climate change in the Tianshan Mountains during the second half of the twentieth century, Clim. Dyn., 46, 303–316, https://doi.org/10.1007/s00382-015-2585-2, 2016.

López-Moreno, J. I., Revuelto, J., Rico, I., Chueca-Cía, J., Julián, A., Serreta, A., Serrano, E., Vicente-Serrano, S. M., Azorín-Molina, C., Alonso-González, E., and García-Ruiz, J. M.: Thinning of the Monte Perdido Glacier in the Spanish Pyrenees since 1981, The Cryosphere, 10, 681–694, http://dx.doi.org/10.5194/tc-10-681-2016, 2016.

Mukupa, W., Roberts, G. W., Hancock, C. M., and Almanasir, K.: A review of the use of terrestrial laser scanning application for change detection and deformation monitoring of structures, Surv. Rev., 1-18, http://dx.doi.org/10.1080/00396265.2015.1133039, 2016.

Mohamed, A., and Wilkinson, B.: Direct georeferencing of stationary lidar, Remote Sens., 1, 1321-1337, http://dx.doi.org/10.3390/rs1041321, 2009.

Nuth, C. and Kääb, A.: Co-registration and bias corrections of satellite elevation data sets for quantifying glacier thickness change, The Cryosphere, 5, 271–290, https://doi.org/10.5194/tc-5-271- 2011, 2011.

Østrem, G. and Brugman, M.: Glacier mass balance measurements: a manual for field and office work. Saskatoon, SK, Environment Canada, National Hydrology Research Institute (NHRI Science Report 4.), 1991.

Paffenholz, J. A., Alkhatib, H., and Kutterer, H.: Direct geo-referencing of a static terrestrial laser scanner, J. Appl. Geod., 4, 115-126, http://dx.doi.org/10.1515/JAG.2010.011, 2010.

Perroy, R. L., Bookhagen, B., Asner, G. P., and Chadwick, O. A.: Comparison of gully erosion estimates using airborne and ground-based LiDAR on Santa Cruz Island, California, Geomorphology, 118, 288–300, http://dx.doi.org/10.1016/j.geomorph.2010.01.009, 2010.

Pieczonka, T. and Bolch, T.: Region-wide glacier mass budgets and area changes for the Central Tien Shan between ~ 1975 and 1999 using Hexagon KH-9 imagery, Global Planet. Change, 128, 1–13, https://doi.org/10.1016/j.gloplacha.2014.11.014, 2015.

Piermattei, L., Carturan, L., and Guarnieri, A.: Use of terrestrial photogrammetry based on structure from motion for mass balance estimation of a small glacier in the Italian alps, Earth Surf. Process. Landforms., 40, 1791 – 1802, http://dx.doi.org/10.1002/esp.3756, 2015.

Revuelto, J., López-moreno, J. I., Azorinmolina, C., Zabalza, J., Arguedas, G., and Vicente-serrano, S. M.: Mapping the annual evolution of snow depth in a small catchment in the Pyrenees using the long-range terrestrial laser scanning, J. Maps, 10, 379-393, http://dx.doi.org/10.1080/17445647.2013.869268, 2014.

Rolstad, C., Haug, T., and Denby, B.: Spatially integrated geodetic glacier mass balance and its uncertainty based on geostatistical analysis: Application to the western Svartisen ice cap, Norway, J. Glaciol., 55, 666–680, https://doi.org/10.3189/002214309789470950, 2009.

RIEGL Laser Measurement Systems: Preliminary Data Sheet, 07.05.2013; Riegl VZ-6000 – 3D Ultra long range terrestrial laser scanner with online waveform processing, RIEGL Laser Measurement Systems, Horn, Austria, 2013.

RIEGL Laser Measurement Systems: 3D terrestrial laser scanner Riegl VZ®-4000/Riegl VZ®-6000 General Description and Data Interfaces, RIEGL Laser Measurement Systems, Horn, Austria, 2014a.

RIEGL Laser Measurement Systems: RiSCAN PRO®–Version 1.8.1, Riegl Laser Measurement Systems, Horn, Austria, 2014b.

Sakai, A. and Fujita, K.: Contrasting glacier responses to recent climate change in high-mountain Asia. Sci. Rep., 7, 13717, https://doi.org/10.1038/s41598-017-14256-5, 2017.

Schnabel, R. and Klein, R.: Octree-based point-cloud compression. In Proceedings of Eurographics Symposium on Point Based Graphics, Boston, MA, USA, 111-120. http://dx.doi.org/10.2312/SPBG/SPBG06/111-120, 2006.

Sold, L., Huss, M., Machguth, H., Joerg, P. C., Leysinger-Vieli, G., Linsbauer, A., Salzmann, N., Zemp, M., and Hoelzle, M.: Mass Balance Re-analysis of Findelengletscher, Switzerland; Benefits of Extensive Snow Accumulation Measurements, Front. Earth Sci., 4, 18, https://doi.org/10.3389/feart.2016.00018, 2016.

Sorg, A., Bolch, T., Stoffel, M., Solomina, O., and Beniston, M.: Climate change impacts on glaciers and runoff in Tien Shan (Central Asia), Nat. Clim. Change, 2, 725–731, https://doi.org/10.1038/NCLIMATE1592, 2012.

Thibert, E., Vincent, C., Blanc, R., and Eckert, N.: Glaciological andVolumetric Mass Balance Measurements: An error analysis over 51 years, Sarennes Glacier, French Alps, J. Glaciol., 54, 522–532, 2008.

Thomson, L. I., Zemp, M., Copland, L., Cogley, J. G., and Ecclestone, M. A.: Comparison of geodetic and glaciological mass budgets for White Glacier, Axel Heiberg Island, Canada, J. Glaciol., 63, 55-66, http://dx.doi.org/10.1017/jog.2016.112, 2017.

Wang, P., Li, Z., Li, H., Wang, W., and Yao, H.: Comparison of glaciological and geodetic mass balance at Urumqi Glacier No. 1, Tian Shan, Central Asia. Global Planet. Change, 114, 14–22. http://dx.doi.org/10.1016/j.gloplacha.2014.01.001, 2014.

Wang, P., Li, Z., Zhou, P., Li, H., Yu, G., Xu, C., and Wang, L.: Long-term change in ice velocity of Urumqi Glacier No. 1, Tian Shan, China, Cold Reg. Sci. Technol., 145, 177-184, http://dx.doi.org/10.1016/j.coldregions.2017.10.008, 2017.

WGMS (World Glacier Monitoring Service): Global Glacier Change Bulletin No.2 (2014–2015), ICSU(WDS)/IUGG(IACS)/UNEP/UNESCO/WMO, World Glacier Monitoring Service, Zurich, Switzerland, 244 pp., publication based on database version, https://doi.org/10.5904/wgms-fog-2017-10, 2017.

Wheaton, J.M., Brasington, J., Darby, S. E., and Sear, D. A.: Accounting for uncertainty in DEMs from repeat topographic surveys: Improved sediment budgets, Earth. Surf. Proc. Land., 35, 136–156, http://dx.doi.org/10.1002/esp.1886, 2010.

Xie, Z. and Liu, C.: Measurement method and main characteristics of the glacier mass balance in Asia. In: Application of Geographic Information Systems in Hydrology and Water Resources (ed. by K. Kovar & H. P. Nachtnabel) (Proc. HydroGIS 93 Conference, Vienna, April 1993), 453–459. IAHS Publ. no. 211, 1991.

Xie, Z. and Liu, C.: Introduction to glaciology. Shanghai Popular Science Press, Shanghai, China, p. 490, 2010, (in Chinese).

Xu, C., Li, Z., Wang, F., Li, H., Wang, W., and Wang, L.: Using an ultra-long-range terrestrial laser scanner to monitor the net mass balance of Urumqi Glacier No. 1, eastern Tien Shan, China, at the monthly scale, J. Glaciol., 63, 792-802, http://dx.doi.org/10.1017/jog.2017.45, 2017.

Young, A. P., Olsen, M. J., Driscoll, N., Flick, R. E., Gutierrez, R., Guza, R. T., Johnstone, E., and Kuester, F.: Comparison of airborne and terrestrial lidar estimates of seacliff erosion in Southern California, Photogramm. Eng. Remote. Sens. 76, 421–427, http://dx.doi.org/10.14358/PERS.76.4.421, 2010.

Yue, X., Zhao, J., Li, Z., Zhang, M., Fan, J., Wang, L., and Wang, P.: Spatial and temporal variations of the surface albedo and other factors influencing Urumqi Glacier No. 1 in Tien Shan, China, J. Glaciol., 63, 899-911, https://doi.org/10.1017/jog.2017.57, 2017.

Zemp, M., Hoelzle, M., and Haeberli, W.: Six decades of glacier mass-balance observations: a review of the worldwide monitoring network, Ann. Glaciol., 50, 101–111, 2009.

Zemp, M., Jansson, P., Holmlund, P., Gärtner-Roer, I., Koblet, T., Thee, P., and Haeberli, W.: Reanalysis of multi-temporal aerial images of Storglaciären, Sweden (1959–99) – Part 2: Comparison of glaciological and volumetric mass balances, The Cryosphere, 4, 345–357, https://doi.org/10.5194/tc-4-345-2010, 2010.

Zemp, M., Thibert, E., Huss, M., Stumm, D., Rolstad Denby, C., Nuth, C., Nussbaumer, S. U., Moholdt, G., Mercer, A., Mayer, C., Joerg, P. C., Jansson, P., Hynek, B., Fischer, A., Escher-Vetter, H., Elvehøy, H., and Andreassen, L. M.: Reanalysing glacier mass balance measurement series, The Cryosphere, 7, 1227–1245, https://doi.org/10.5194/tc-7-1227-2013, 2013.

Zemp, M., Frey, H., Gärtner-Roer, I., Nussbaumer, S. U., Hoelzle, M., Paul, F., Haeberli, W., Denzinger, F., Ahlstrøm, A. P., Anderson, B., Bajracharya, S., Baroni, C., Braun, L. N., Cáceres, B. E., Casassa, G., Cobos, G., Dávila, L. R., Delgado Granados, H., Demuth, M. N., Espizua, L., Fischer, A., Fujita, K., Gadek, B., Ghazanfar, A., Hagen, J. O., Holmlund, P., Karimi, N., Li, Z., Pelto, M., Pitte, P., Popovnin, V. V., Portocarrero, C. A., Prinz, R., Sangewar, C. V., Severskiy, I., Sigurdsson, O., Soruco, A., Usubaliev, R., and Vincent, C.: Historically unprecedented global glacier decline in the early 21st century, J. Glaciol., 61, 745–762, https://doi.org/10.3189/2015JoG15J017, 2015.

Zhang, Z.Y.: Iterative point matching for registration of free-form curves, Int. J. Comput. Vision., 13, 119–152, http://dx.doi.org/10.1007/BF01427149, 1992.

The Cryosphere Discuss., https://doi.org/10.5194/tc-2018-128
Manuscript under review for journal The Cryosphere
Discussion started: 7 August 2018

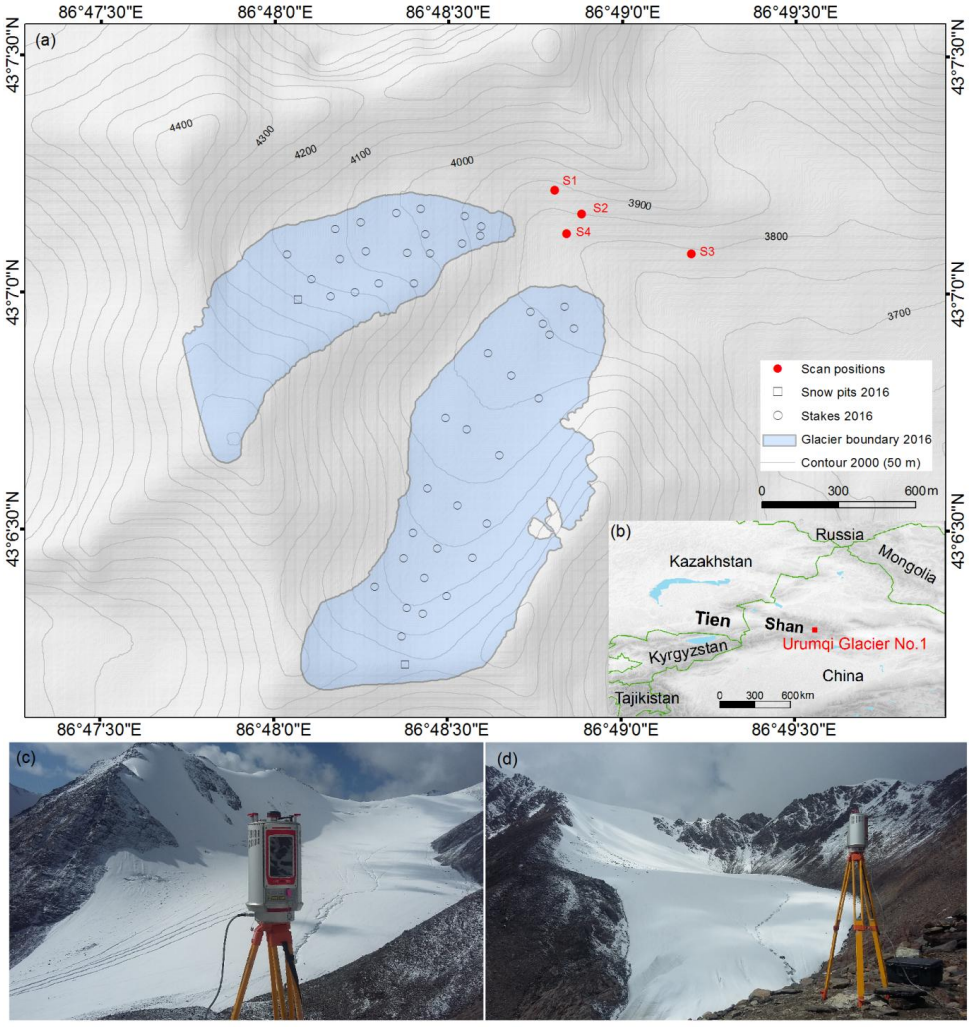

Figure 1. Overview of the study area. (a) The glaciological mass balance measuring network in 2016; glacier boundary delineated from TLS-derived DEM (1 September 2016). Also depicted are the locations of four scan positions. (b) Location map of UG1 in eastern Tien Shan. (c) Riegl VZ®-6000 TLS survey of EB at scan position S2 and (d) TLS survey of WB at scan position S1 (27 August 2017).

The Cryosphere Discuss., https://doi.org/10.5194/tc-2018-128
Manuscript under review for journal The Cryosphere
Discussion started: 7 August 2018

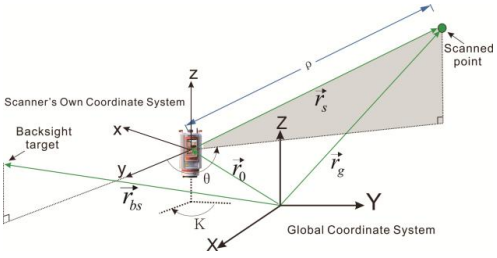

Figure 2. TLS observables and direct georeferencing.

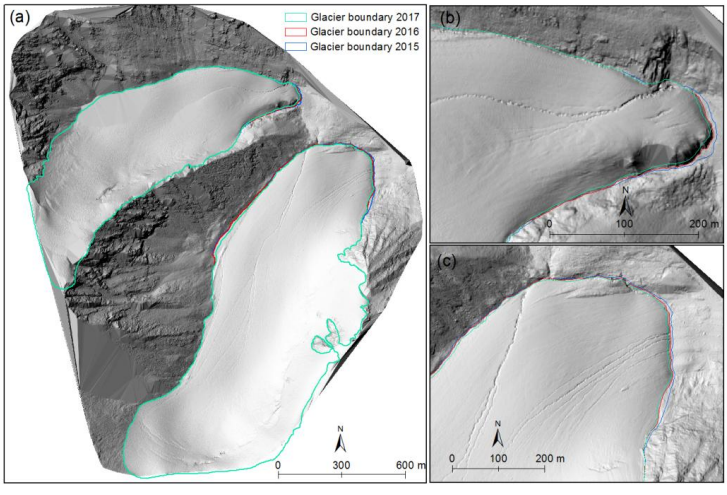

Figure 3. (a) Shaded reliefs of UG1 margin calculated based on the TLS-derived DEM (on 1 September 2016) with the glacier boundary 2015 (blue), 2016 (red) and 2017 (green). Glacier terminus variations of WB (b) and EB (c) are also shown.

The Cryosphere Discuss., https://doi.org/10.5194/tc-2018-128
Manuscript under review for journal The Cryosphere
Discussion started: 7 August 2018

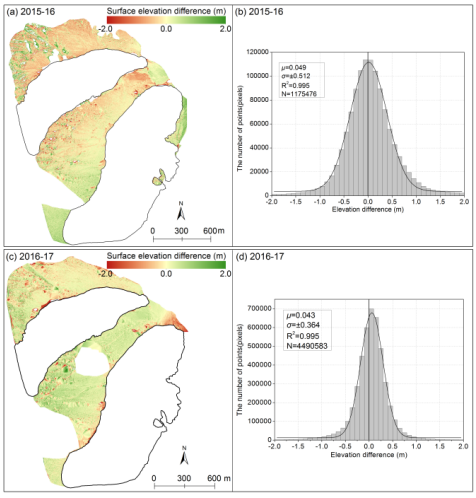

Figure 4. Statistics on annual surface elevation changes over stable terrain extracted by differencing of TLS-derived DEMs from two consecutive years. Spatial and corresponding frequency distributions of these changes for 2015-16 (a, b) and 2016-17 (c, d). The median (μ) and the standard deviation (σ) of the elevation differences and the number of pixels (N) off glacier are given.

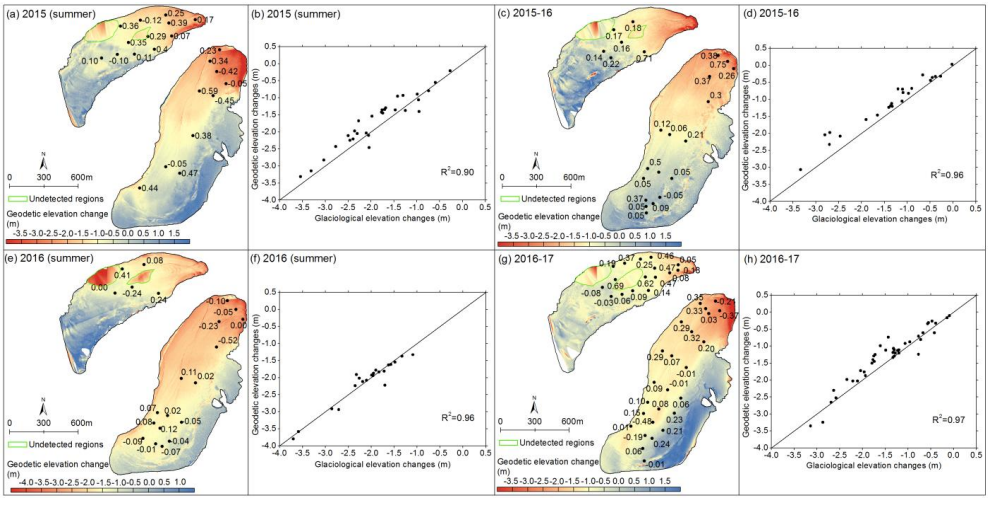

Figure 5. Spatial distribution of TLS-derived glacier surface elevation changes (a, c, e and g); the numbers represent the differences (the unit is m) between the TLS-derived (Δh_{TLS}) and glaciological in situ measured (Δh_{glac}) elevation changes at corresponding ablation stakes (Δh_{TLS} - Δh_{glac}). Scatter plots of glaciological elevation change against geodetic elevation change at corresponding ablation stakes are presented, and the quality of fittings in terms of R^2 is also presented (b, d, f and h). Black lines are TLS-derived glacier boundary of UG1 and same as the corresponding boundary of Figure 3. White areas indicate outliers, which we have deleted. Two green polygons indicate artefacts that have not been detected by the TLS.

The Cryosphere Discuss., https://doi.org/10.5194/tc-2018-128
Manuscript under review for journal The Cryosphere
Discussion started: 7 August 2018

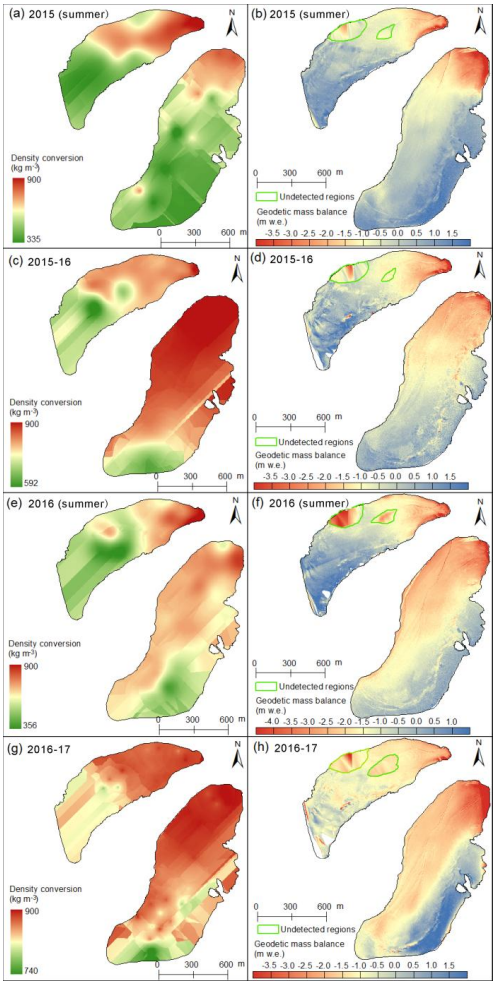

Figure 6. Distributed density conversions (a, c, e and g) and corresponding glacier-wide geodetic mass balance (b, d, f and h). Two green polygons indicate artefacts that have not been detected by the TLS. Black lines are same as the corresponding boundary of Figure 3.

The Cryosphere Discuss., https://doi.org/10.5194/tc-2018-128
Manuscript under review for journal The Cryosphere
Discussion started: 7 August 2018

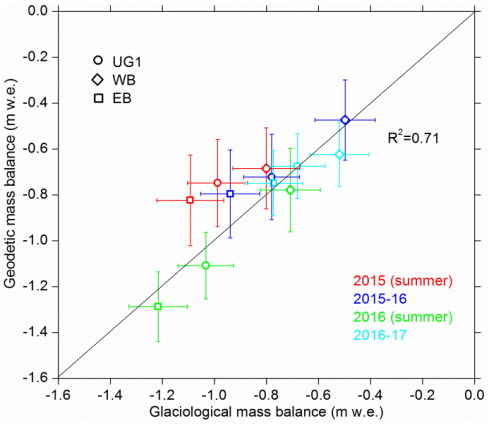

Figure 7. Glaciological versus TLS-derived geodetic mass balances for Urumqi Glacier No.1 (UG1), the west branch (WB) and the east branch (EB), with errors bars for two independent methods.

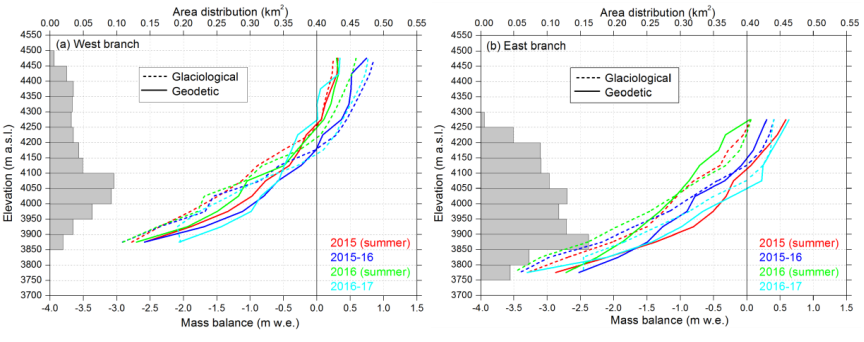

Figure 8. The hypsometry (50 m altitudinal ranges, see Figure 10) and the glaciological (dotted line) and geodetic (solid line) mass balance elevation distribution for the whole study period; both summer and annual mass balances are shown. Gray horizontal bars indicate the area-elevation distribution of UG1.

The Cryosphere Discuss., https://doi.org/10.5194/tc-2018-128
Manuscript under review for journal The Cryosphere
Discussion started: 7 August 2018

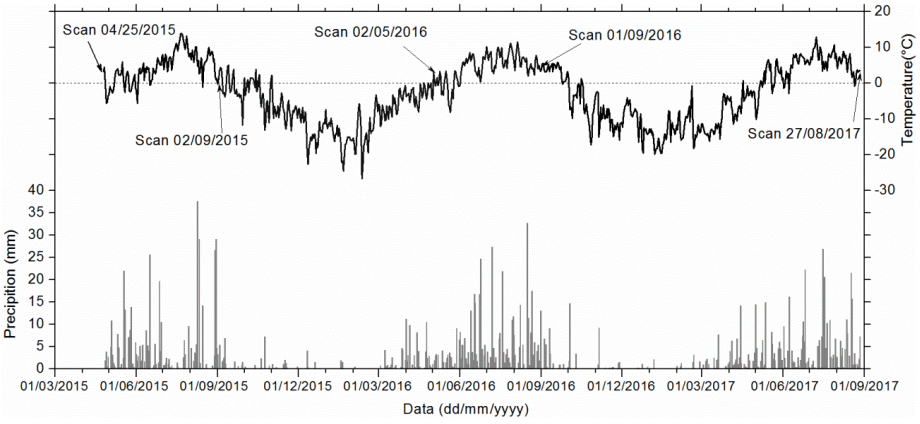

Figure 9. Daily precipitation and mean temperature observed at the DMS during 25 April 2015 - 28 August 2017.

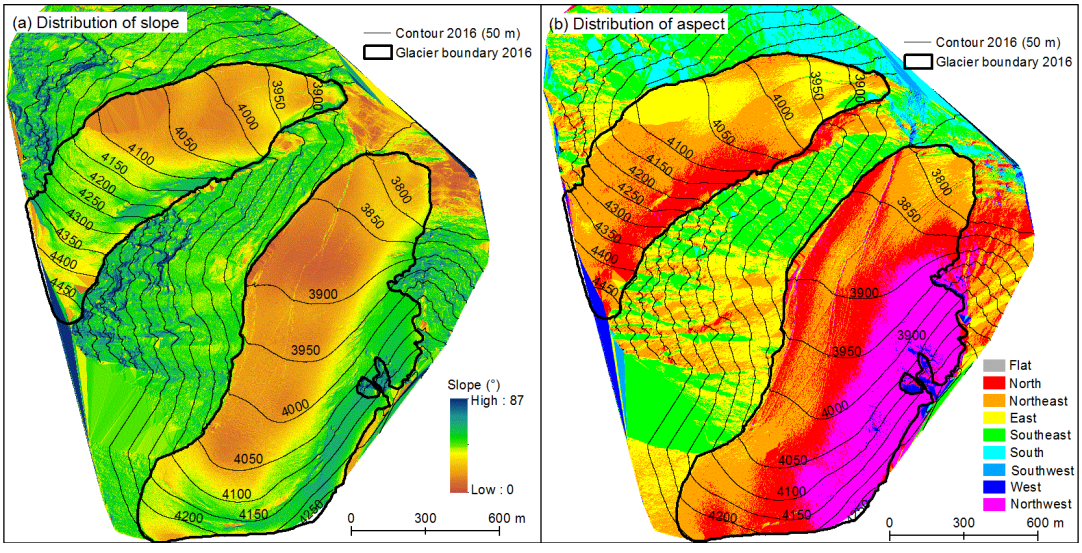

Figure 10. Spatial distributed slope (a) and aspect (b) of UG1 extracted from TLS-derived DEM on 1 September 2016.

The Cryosphere Discuss., https://doi.org/10.5194/tc-2018-128
Manuscript under review for journal The Cryosphere
Discussion started: 7 August 2018

Table 1. Parameters and values of Riegl VZ®-6000 terrestrial laser scanner (RIEGL Laser Measurement Systems, 2014a).

System parameter	Parameters and values (range performance)			
Laser pulse repetition rate (kHz)	30	50	150	300
Effective measurement rate (meas./sec)	23 000	37 000	113 000	222 000
Max. measurement range (m):				
- natural targets $\rho \geq 90\%$	6000	6000	4200	3300
- natural targets $\rho \geq 20\%$	3600	3600	2400	1800
Accuracy (mm)	15	15	15	15
Precision (mm)	10	10	10	10
Minimum range (m)	5			
Temperature range (℃):				
- operation	0 to 40			
- storage	-10 to 50			
Vertical and horizontal angle measurement resolution (°)	better than 0.0005			

Table 2. Riegl VZ®-6000 TLS surveying parameters of UG1.

Date dd/mm/yyyy	Scanning range* (with overlap) m^2	Number of points	Average point density points m^{-2}	Vertical angle resolution °	horizontal angle resolution °	Total scan time min
25/04/2015	3 204 684	12 740 500	3.98	0.020	0.020	46
02/09/2015	4 707 863	65 500 749	13.91	0.019/0.046	0.019/0.046	103
02/05/2016	3 224 285	26 908 210	8.35	0.020	0.020	82
01/09/2016	3 316 262	42 354 299	12.77	0.020	0.020	101
27/08/2017	3 161 489	54 835 821	17.34	0.020	0.020	88

*Scanning range is the total areas of four scan positions and does not include overlapped areas. The overlap percentage of the four scans on 25 April 2015 is smaller than other scan campaigns so that the average point density is relatively low.

The Cryosphere Discuss., https://doi.org/10.5194/tc-2018-128
Manuscript under review for journal The Cryosphere
Discussion started: 7 August 2018

Table 3. Error or StdDev (σ_{MSA}) (in m) of Multi-Station Adjustment (MSA) and the number of points (n) used for multi-temporal registration of two consecutive campaigns. The mean (μ) and the standard error ($\sigma_{\overline{\Delta h TLS}}$) are calculated based on the elevation changes over stable terrain (in m).

Period*	σ_{MSA}	n	μ	$\sigma_{\overline{\Delta h TLS}}$
2015 (summer)	0.278	11 214 842	-0.014	0.250
2015-16	0.065	10 182 829	0.049	0.229
2016 (summer)	0.195	10 486 985	-0.005	0.216
2016-17	0.072	18 657 232	0.043	0.163

* 2015 (summer) = 25 April –2 September 2015; 2015-16 = 2 September 2015 – 1 September 2016; 2016 (summer) = 2 May – 1 September 2016; 2016-17 = 1 September 2016 – 27 August 2017.

Table 4. Glacier-wide mean of density conversion (ρ) and its uncertainty (σ_ρ) (in kg m^{-3}) as well as TLS-derived glacier surface elevation changes ($\overline{\Delta h TLS}$) (in m). TLS-derived geodetic (B_{geod}) and in situ measured glaciological (B_{glac}) net mass balance at winter and annual scales are listed (in m w.e.).

Period	ρ	σ_ρ	$\overline{\Delta h TLS}$	B_{geod}	B_{glac}
2015 (summer)					
UG1	752	34	-0.991	**-0.748 ±0.190**	**-0.988 ±0.115**
WB	696	35	-1.014	-0.684 ±0.177	-0.801 ±0.129
EB	782	33	-0.952	**-0.824 ±0.197**	**-1.093 ±0.128**
2015-16					
UG1	810	21	-0.827	-0.722 ±0.186	-0.780 ±0.107
WB	763	24	-0.625	-0.474 ±0.175	-0.498 ±0.116
EB	837	20	-0.873	**-0.796 ±0.192**	**-0.939 ±0.113**
2016 (summer)					
UG1	622	32	-1.654	-1.109 ±0.145	-1.033 ±0.107
WB	579	34	-1.230	-0.779 ±0.132	-0.708 ±0.115
EB	647	31	-1.925	-1.288 ±0.152	-1.216 ±0.112
2016-17					
UG1	864	19	-0.746	-0.675 ±0.141	-0. 681 ±0.107
WB	861	19	-0.844	-0.749 ±0.141	-0.773 ±0.113
EB	865	19	-0.729	-0.624 ±0.142	-0.519 ±0.112